

Compact and efficient quantum frequency conversion of a fiber-pigtailed single-photon source

Mathis Cohen¹, Anthony Martin¹, Romain Dalidet¹, Florian Pastier², Marie Billard², Aristide Lemaitre³, Valérian Giesz², Niccolo Somaschi², Sarah Thomas³, Pascale Senellart-Mardon³, Sébastien Tanzilli¹, Laurent Labonté^{1*}

¹Université Côte d'Azur, CNRS, Institut de physique de Nice, France

²Quandela SAS, Palaiseau, France and

³Université Paris-Saclay, CNRS, Centre de Nanosciences et de Nanotechnologies (C2N), Palaiseau, France

Quantum frequency converters are key enabling technologies in photonic quantum information science to bridge the gap between quantum emitters and telecom photons. Here, we report a coherent frequency converter scheme combining a fiber-coupled nonlinear optical Lithium Niobate waveguide with a fiber-pigtailed single-photon source based on semiconductor quantum dots. Single and indistinguishable photons are converted from 925.7 nm to the telecommunication C-band, with a 48.4% end-to-end efficiency and full preservation of single-photon purity and indistinguishability. The integration of the two fiber-based modules achieving top-level performance represents an important step toward the practical interconnection of future quantum information processing systems operating at different wavelengths.

I. INTRODUCTION

Distributing quantum resources over long-distance optical fiber networks is currently a challenge [40]. This has already allowed quantum nonlocality to be demonstrated in a wide variety of applications, including device-independent quantum key distribution [59, 60], deterministic quantum teleportation [36], entanglement-based clock synchronisation [35, 55], distributed quantum sensors [53], and quantum repeaters [56]. The latter approach appears to be a viable solution for transferring photonic quantum states from one location to another. A major challenge relies on the incompatibility in terms of the wavelength between telecom photons (~ 1550 nm), which represent natural flying qubit carriers for establishing entanglement, and deterministic single-photon emitters (nodes based on atoms, semiconductor quantum dots, or colour centres) that mainly operate in the near-infrared (NIR) range ($\sim 780 - 950$ nm). Quantum frequency conversion (QFC) addresses this challenge by bridging the gap between distinct spectral ranges by transferring the wavelength of a photonic state to another while preserving its quantum properties. QFC also presents an alternative solution for establishing true single-photon emission at telecommunication wavelengths, as the typical emission wavelength of mature single-photon emitters lies in the NIR range ($\sim 900 - 950$ nm) [52]. As such, QFC has received a lot of attention over the past years through the demonstration of photonic quantum information downconverters [45, 74, 77], matter-light entanglement [11, 66–72], quantum storage of entangled telecom-wavelength photons [73], as well as bright and pure single-photon source at telecom wavelength [61, 63–65, 75, 76].

QFC relies on nonlinear processes, such as sum-frequency generation (SFG) or difference-frequency generation

(DFG), typically driven by strong pump fields to facilitate spectral translation across hundreds of nanometers. Although numerous experimental demonstrations have been carried out in free-space configurations [11, 12, 65] that offer excellent control of spatial modes and filtering capabilities, they often lack scalability and operational robustness, making them impractical for out-of-lab deployment. Recent efforts have aimed at developing integrated or fiber-compatible platforms to overcome these limitations. Chip-scale approaches using micro-ring resonators in GaAs or silicon photonics [8–10, 18] offer a high degree of miniaturization and potential CMOS compatibility. However, these systems tend to operate over narrow spectral windows, are sensitive to fabrication variations, and often suffer from limited external efficiency owing to the challenging fiber coupling and tight phase-matching constraints. For full system integration, it remains essential to focus on practical issues such as coupling losses, noise, and packaging. Fiber-pigtailed waveguides, such as PPLN modules, offer a valuable compromise between efficiency and integration [23], although the preservation of quantum properties and the overall system efficiency still leaves room for improvement. In this study, we focus on the conversion of photons emitted around 900 nm [52, 75, 76], as this wavelength is at the crossroads of the most performing quantum dots (QD) [52] and other solid-state emitters, such as SiC [62], envisioning true single-photon emission and quantum repeater-based networks operating in the telecom range. We present a fiber-based QFC system that leverages fiber-to-chip coupling and achieves a high overall efficiency 48.4 % from 925 to 1560 nm. It operates on a commercial fiber-pigtailed single photon source based on QDs [3]. We demonstrate the full preservation of the unicity and indistinguishability of single photons produced by a QD, with $g^{(2)}(0) = 0.044(1)/0.051(1)$ and indistinguishability = 79.3(3)%/80.0(8)% before and after conversion, respectively. Finally, by leveraging a tunable pump laser, we demonstrate the flexibility of the conver-

* laurent.labonte@univ-cotedazur.fr

sion process over a 10 nm range, enabling the alignment of the telecom wavelengths of converted single photons originating from different QDs, a common scenario in realistic quantum networks.

II. EXPERIMENT

A. Single-photon source and conversion modules

The experimental setup for the QFC is shown in Fig. 1. The conversion interface can be divided into three stages. In the signal stage, a picosecond Ti:Sa laser (76 MHz repetition rate) is utilized to pump a fiber-pigtailed single-photon source based on a self-assembled InGaAs quantum dot embedded in an optical cavity. The polarisation and power of the pulses were meticulously controlled using half-wave plates (HWP) and a polarisation beam splitter (PBS). The QD is embedded within a micropillar structure composed of distributed Bragg reflectors fabricated using an advanced in situ lithography technique [51]. A single-mode fiber (SMF) is precisely positioned on top of the micropillar at room temperature, with nanometer scale accuracy, maintained from 300 K to 7 K [3]. The complete system developed by *Quandela* is fully operational and integrated. It comprises a pulse-shaping stage designed to ensure optimal matching between the cavity mode and spectral bandwidth of the excitation pulse, followed by injection into the fibered source maintained at 7 K within a closed-cycle cryostat. The source was operated with a 0.7 nm blue detuned laser exploiting the phonon-assisted excitation scheme [2]. The final stage involves the collection of single photons at a wavelength of $\lambda_{SP} = 925.7$ nm, with band-pass filters (BPF) employed to eliminate residual excitation laser light at $\lambda_{exc} = 925.0$ nm.

The conversion stage is devoted to the frequency conversion process through difference-frequency generation (DFG). This nonlinear effect occurs within a 4 cm long periodically poled Lithium Niobate waveguide (PPLN/WG) with a poling period of $\Lambda = 25.45 \mu\text{m}$. The waveguide is specifically designed with a poling period tailored for wavelength conversion from 925.7 nm to 1560 nm, ensuring compliance with both energy conservation and quasi-phase-matching conditions:

$$\left\{ \begin{array}{l} \omega_{sig} - \omega_{pump} = \omega_{conv}, \\ \mathbf{k}_{sig} - \mathbf{k}_{pump} + \frac{2\pi}{\Lambda} \mathbf{n} = \mathbf{k}_{conv}, \end{array} \right. \quad (1)$$

where Λ is the poling period of the crystal and \mathbf{n} is a unitary vector.

A pump laser beam at 2272 nm is employed to satisfy the required conditions for frequency conversion and constituted the pump stage. The laser operating in continuous wave mode (CW) is also injected into the SMF. Appropriate optical components are employed to control the polarisation and mitigate photonic noise.

The conversion stage is fully fiber-integrated. A 980/1560 nm wavelength demultiplexer is used to combine the signal and pump beams into the waveguide. For alignment, the output fiber is cleaved and positioned with a 3-axis micrometric mount placed less than 1 mm from the waveguide facet. Thanks to the large waveguide cross-section (12 $\mu\text{m} \times 12 \mu\text{m}$), the near-perfect mode matching between the waveguide and the fundamental spatial mode of the signal, together with the anti-reflection coating, enables a high coupling efficiency (88%) at the signal wavelength without requiring microlenses. In contrast, the pump beam exhibits a spatially multimode profile, which leads to suboptimal coupling into the WG (55% efficiency). These injection losses are compensated by using a high pump power to reach maximal conversion efficiency. The converted photons are collected with a standard telecom fiber (SMF28) at 1560 nm, aligned using the same method as for the input. Coupling optimization is performed in the classical emission regime by replacing the SPS with a 925 nm CW laser. A filtering stage composed of four telecom dense-wavelength demultiplexers (DWDM) is used to achieve a high extinction of residual pump photons and non-converted single photons.

B. Phase-matching

The phase-matching bandwidth should exceed the spectral width of the photons, which is approximately $\Delta\lambda_{SP} \simeq 4 \text{ pm}$, to achieve complete conversion, but also cover a wider conversion range for more flexibility. To test our QFC, we perform measurements in the classical regime by substituting the QD with a CW laser tuned to approximately 925 nm. The primary tunable parameter that influences the phase-matching width is crystal temperature. The PPLN crystal is mounted on an oven connected to a temperature controller, which allows for precise stabilisation and temperature adjustment. A linear drift is performed, and the converted signal is detected using a photodiode. Fig. 1(b) shows the resulting signal, from which the full width at half maximum (FWHM) of the central lobe is extracted. We achieve $\text{FWHM}_{NIR} = 0.40 \pm 0.02 \text{ nm}$ at $\lambda_{NIR} = 925.0 \text{ nm}$ at a temperature of $T_{PPLN} = 43.4^\circ\text{C}$, satisfying the condition of $\text{FWHM}_{NIR} \gg \Delta\lambda_{SP}$.

To further optimise the system, we conduct phase-matching measurements to ensure that our conversion interface could accommodate wavelength mismatches from different single-photon sources. By adjusting the central wavelengths of the pump beam and modifying the temperature of the PPLN crystal, we maintain phase-matching centred at 1560 nm. The phase-matching bandwidth remains the same while varying the wavelength of the signal photons from 920 to 930 nm (Fig. 2 a-d), with FWHM_{NIR} between 0.37 nm and 0.49 nm, which are still lower than the spectral width of the photons. The crystal used in this setup features six waveguides with different

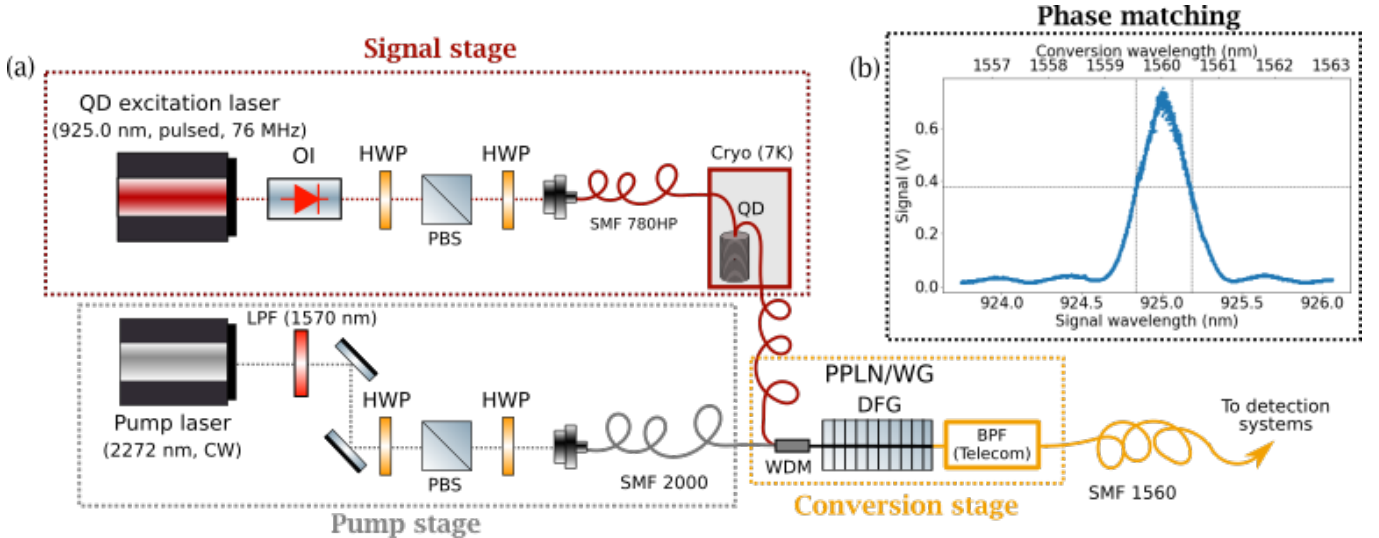


FIG. 1: (a) Experimental setup of the frequency conversion interface. The signal and pump beams are going through the HWP and PBS to control the polarisation and power. The SMF are used to clean the spatial modes. Overlapping is performed using a WDM coupled into the PPLN/WG. The dashed lines correspond to free-space propagation. We filter the converted photons using telecom DWDM. (b) Phase matching of conversion process with $T_{PPLN} = 43.4^\circ\text{C}$. FWHM are extracted, for the signal (FWHM_{NIR} = $0.40 \pm 0.02 \text{ nm}$) and the conversion (FWHM_{conv} = $1.00 \pm 0.02 \text{ nm}$).

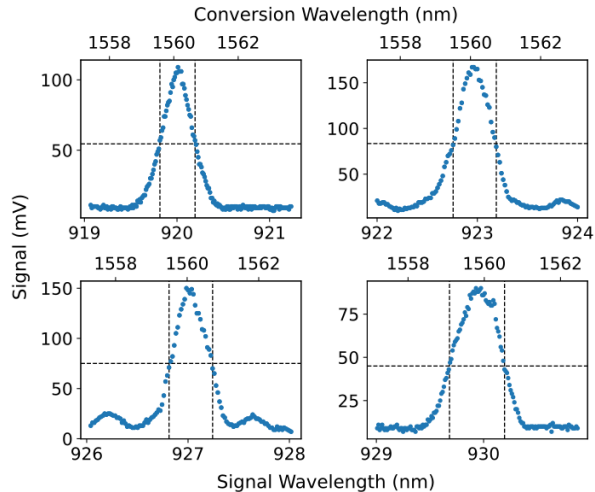


FIG. 2: Phase matching curves with different central signal wavelength. The temperature is adjusted to conserve the central conversion wavelength of 1560 nm. For these four curves: $0.37 \text{ nm} < \text{FWHM}_{\text{NIR}} < 0.49 \text{ nm}$, with the PPLN temperature from 33.0°C to 82.5°C .

poling periods, extending the spectral tuning range to approximately 60 nm. This range ensures the compatibility of the interface with various single-photon source technologies.

C. Efficiency

The conversion efficiency is a key factor in evaluating the performance of the QFC interface. To determine the maximum achievable efficiency of a single photon from the QD, we measure the performance for various levels of coupled pump power in the waveguide. A superconducting nanowire single-photon detector (SNSPD) operating in the telecom band is employed to detect the number of converted photons at the output of the QFC. The external conversion efficiency, η_{ext} , is calculated by comparing the number of signal photons injected into the conversion interface, $N_{\text{sig}}^{\text{in}}$, with the number of converted photons at the output, $N_{\text{conv}}^{\text{out}}(P_{\text{pump}})$, as a function of the pump power:

$$\eta_{\text{ext}} = \frac{N_{\text{conv}}^{\text{out}}(P_{\text{pump}})}{N_{\text{sig}}^{\text{in}}}. \quad (2)$$

Fig. 3 shows our results compared with the theory described by the following formula:

$$\eta(P_{\text{pump}}) = \eta_{\text{max}} \sin^2 \left(L \sqrt{\eta_n P_{\text{pump}}} \right), \quad (3)$$

where η_{max} , P_{pump} , L and η_n are the maximum conversion efficiency, coupled pump power, length of the non-linear media, and normalised efficiency specific to the device, respectively.

The theoretical efficiency of DFG is subject to an optimal value, as excessive pump power can lead to reconversion processes that limit the efficiency. We achieve

a maximum external conversion efficiency of $\eta_{ext,max} = 48.4\%$ with a coupled pump power of $P_{pump} = 285\text{ mW}$.

At then input of the QFC stage, the in-fiber single-photon rate is 2.8 MHz, corresponding to 3.7 % brightness. After frequency conversion at the maximum efficiency, the converted photon rate is 1.3 MHz. The discrepancy between the experimental data and theoretical curve is attributed to the noise generated during the conversion process, primarily from two sources: Raman scattering and residual pump light. The filtering stage has been optimized to maintain high brightness while minimising the noise contribution. To assess noise performance, we measure the signal-to-noise ratio (SNR) by comparing detections inside and outside the phase-matching range of the conversion. In the optimal regime ($P_{pump} = 285\text{ mW}$), the SNR exceeds 400, demonstrating the effective noise suppression and high performance of the conversion interface.

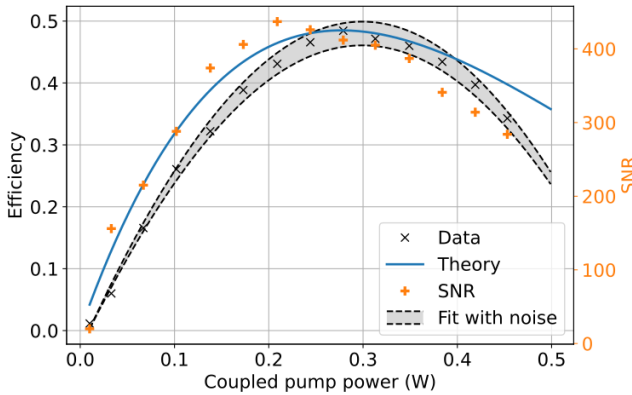


FIG. 3: External conversion efficiency as a function of coupled pump power. The data (black) are fitted (grey zone) and compared with the theoretical curve (blue). Orange dots : Signal-to-noise ratio of the interface, depending on the coupled pump power.

D. Unicity & indistinguishability

We now compare the properties of the single photons before and after passing through the conversion interface. The initial characterisation focuses on the unicity (or single-photon purity) of the source and quantifies the probability of emitting more than one photon per pulse. The relevant parameter is the second-order autocorrelation coefficient at zero delay $g^{(2)}(0)$, which is defined as

$$g^{(2)}(0) = \frac{\langle \hat{n}(\hat{n} - 1) \rangle}{\langle \hat{n} \rangle^2}, \quad (4)$$

where \hat{n} denotes the photon-number operator. To measure this parameter, we utilize two Hanbury-Brown and Twiss (HBT) interferometers, one in the NIR band and

the other in the telecom band. Each interferometer is configured with a 50/50 beam splitter (BS), two detectors, and a time tagger to record coincidence events (Fig. 4). Coincidence histograms are generated as a function of the delay between detectors. To extract the values of $g^{(2)}(0)$, we compare the area of the zero-delay peak with the mean area of the other peaks, which correspond to correlations between successive photons. This comparison is made using the following formula.

$$g^{(2)}(0) = \frac{A_0}{\frac{1}{N} \sum_{n \neq 0} A_n}, \quad (5)$$

with $A_{0,...,n}$ peak area at delays 0, ..., n and N total peak numbers. Histograms are shown in the upper row of Fig. 4, highlighting a reduction in coincidences at zero delay. We measure $g^{(2)}(0)_{NIR} = 0.044(1)$ and $g^{(2)}(0)_{Tel} = 0.051(1)$ before and after the conversion, respectively, indicating good preservation of the single-photon purity. Note that the single-photon purity in this experiment was probably limited by the non-optimal laser filtering stage. A higher single-photon purity can be achieved with $g^{(2)}(0)$ values below 10^{-2} with optimised excitation schemes and filtering [50].

The second step involves characterising the indistinguishability between single photons consecutively emitted by the QD. Indistinguishability here means that the photons are identical in all modes, including polarisation, temporal, spatial, and spectral modes. To quantify this, we conduct a Hong-Ou-Mandel (HOM) experiment involving two-photon interference between consecutive photons. In the HOM experiment, two indistinguishable photons are sent into a 50/50 beam splitter (BS), leading to a dip in the coincidence histogram at zero delay, known as the HOM dip. The visibility of this interference, V_{HOM} , provides a measure of the indistinguishability of photons emitted by the QD. To demonstrate this property, we set up an unbalanced Mach-Zehnder interferometer (UMZI) with a relative delay corresponding to the repetition rate of the QD excitation laser (76 MHz, equivalent to 13 ns). Two UMZIs are constructed, one for the NIR band and one for the telecom band, with a free-space section to finely adjust the relative delay. The photons are prepared in a diagonal polarisation state and separated by a polarisation beam splitter (PBS) at the input of the interferometer. SNSPDs are used to detect photons and coincidence events are recorded using a time-to-digital converter (TDC). To evaluate V_{HOM} , we compare the coincidence counts when the photons are maximally distinguishable and when they are indistinguishable. The polarisation mode is adjusted using an HWP to prepare photons with either co- or cross-polarisation. The visibility is extracted using the following formula:

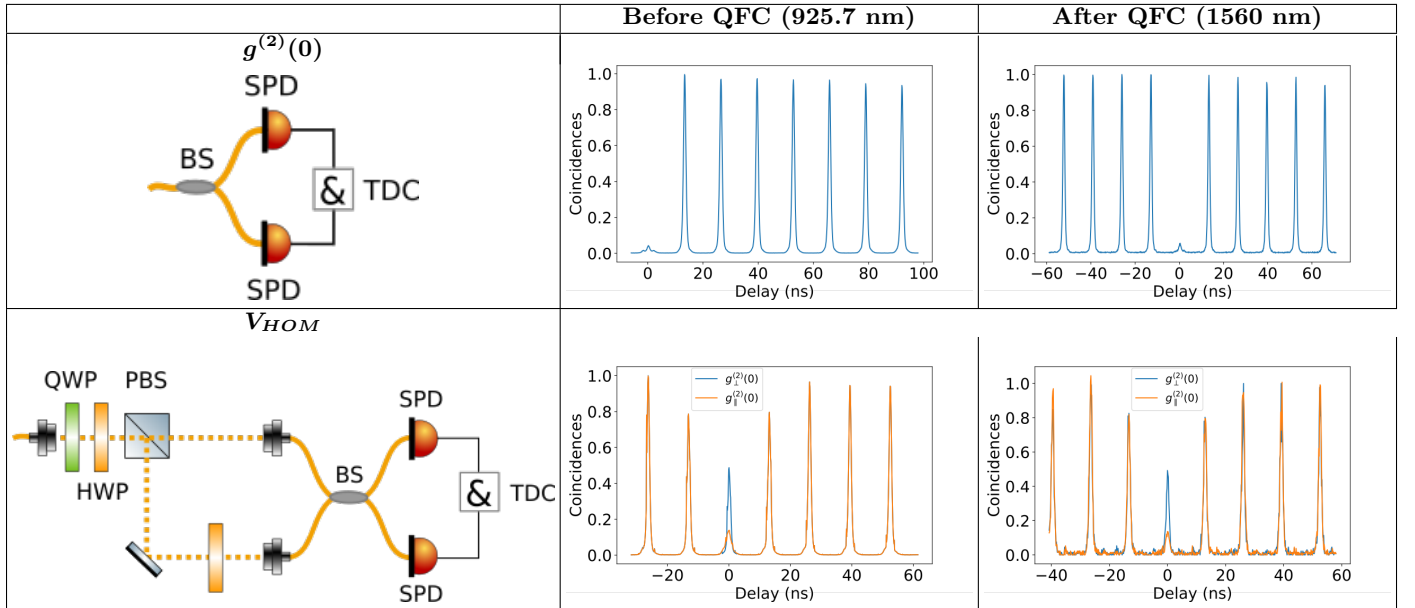


FIG. 4: Characterization of single photon properties conservation. *Left column* : Detection setups. $g^{(2)}(0)$ is measured using an HBT interferometer, recording coincidences on a time-to-digital converter (TDC) and receiving signals from single-photon detectors (SPD). The V_{HOM} is extracted by using an UMZI, using a HWP to configure indistinguishable case (co-polarization) and distinguishable case (cross-polarization). *Middle column* : Results in NIR band, at the output of the QD. *Right column* : Results after conversion, at 1560 nm.

III. DISCUSSION

$$V_{HOM} = 1 - \frac{g_{\parallel}^{(2)}(0)}{g_{\perp}^{(2)}(0)}, \quad (6)$$

with $g_{\parallel(\perp)}^{(2)}(0)$ zero-delay coincidence peak for the indistinguishable (distinguishable) case. This raw value is corrected to obtain the single-photon indistinguishability (M_s), correcting for accidental coincidences caused by the nonzero $g^{(2)}(0)$ of the source [49]:

$$M_s = \frac{V_{HOM} + g^{(2)}(0)}{1 - g^{(2)}(0)}. \quad (7)$$

We compare the results before and after the conversion interface by measuring the areas of the zero-delay peaks. For the raw data, we obtain $V_{HOM}^{NIR} = 71.4(3)\%$ and $V_{HOM}^{Tel} = 70.8(8)\%$, indicating ideal preservation of indistinguishability. After applying the corrections, the indistinguishability values are $M_s^{NIR} = 79.3(3)\%$ and $M_s^{Tel} = 80.0(8)\%$ before and after conversion, respectively. The non-ideal indistinguishability of the source under study arises from the low Purcell factor experienced by the source in the low-quality factor cavity. These results underscore the effective coherence preservation achieved using the conversion interface.

The characterization of the QFC interface is summarized in Table I. We now compare our results with state-of-the-art interfaces based on the DFG process for single-photon conversion from the NIR to telecom band. We first highlight the performance of our QFC independently of the SPS, because our QFC can be adapted to any SPS. Our QFC demonstrates the highest end-to-end conversion efficiency of approximately 900 nm while preserving the unicity and indistinguishability properties of the SPS. Additionally, the spectral tunability of our scheme, which leverages the PPLN crystal and pump laser, offers significant flexibility for interfacing with a multitude of NIR SPS, allowing for the integration of dissimilar SPS. A key distinction of our approach is the advantageous use of optical fiber components throughout the interface. Single photons are collected in a fiber and transmitted to a fully fibered conversion stage, maintaining a high coupling efficiency and generating minimal losses. The fiber-based system provides notable compactness, with the pump preparation, conversion, and filtering stages mounted on a 400×400 mm breadboard, enhancing transportability and making the setup suitable for real-world applications. While reference [46] reports a higher internal efficiency, their setup involves a more complex fiber connection, which poses challenges for integration with standard SMF28 fibers or other common systems. This complexity may hinder practical deployment and integration compared with our more

Work	λ_{NIR}	QFC $\eta_{max,ext}$	$g^{(2)}(0)$	NIR/TC	M_s NIR/TC	SP rate NIR/TC	Inj./Coll. QFC
This work	925 nm	48.4 %	4.4/5.1 %	79.3/80.0 %	2.8/1.3 MHz	fully fiber-coupled	
Da Lio et al. [75]	945 nm	40.8 %	2.0/2.4 %	93.5/94.8 %	2.21/0.905 MHz	partially fiber-coupled	
Morrison et al. [76]	942 nm	35 %	4.0/4.3 %	95/67 %	1.46/0.456 MHz	partially fiber-coupled	
Rickert et al. [27]	1550 nm	No conversion	-/ < 4 %	-/79-(55) %	-/0.6-(1.2) MHz	fully fiber-coupled	

TABLE I: Comparison of this work with similar QFC at the state-of-the-art. Efficiencies are reported fiber-to-fiber. The coupling scheme indicates whether the PPLN stage is fully fiber-coupled or includes a free-space interface. The last line represents the current state-of-the-art in the direct generation of a telecom single-photon source with QDs [27]. Two numbers are those reported, the higher (lower) indistinguishability being reported for half (full) brightness.

streamlined and transportable fiber-based approach.

Table I further highlights that the single-photon source performance obtained at the end of the QFC system represents a new record value in terms of the photon rate. We note that this is achieved for the very first time using a commercial fiber-pigtailed source, where recent progress has shown a factor of six increase in fibered brightness in the NIR [3]. The direct generation of single photons in the telecom band from QDs has attracted significant interest in recent years [1, 4, 5, 27, 34, 42–44], achieving a promising performance in terms of unicity and indistinguishability. Notably, the recent work in [4] which we include in Table I, illustrates significant advances in these metrics with, for the first time, a photon indistinguishability of 79 % at 0.6 MHz. These values represent important progress, approaching for the first time the performance of the best NIR SPS converted to the telecom band. However, we note that the QFC is an important asset for bringing the capability of NIR QD sources to generate spin-photon entanglement [37–39] into the telecom range for quantum networks and distributed optical quantum computing.

Improvements to the QFC interface are envisioned to enhance performance and operational usage. The principal source of loss is the filtering stage after conversion, which corresponds to -0.8 dB owing to several DWDMs connected in series. A strong pump beam can be better suppressed with custom fiber optics featuring a high extinction ratio tailored to our specific wavelengths. Additionally, the non-ideal coupling of the signal with cleaved fibers in the waveguide (currently at 88%) can be improved through pigtailing techniques. Furthermore, the internal efficiency of the PPLN has been characterized in the classical regime to estimate the total achievable efficiency by measuring $\eta_{int} \sim 66\%$. The non-unity internal efficiency is mainly due to the spatial mode mismatch between the signal and the fundamental mode of the waveguide. QFC developed using Lithium Niobate on insulator (LNOI) have achieved higher internal efficiencies and hold promise for integration through nanophotonics chips [48].

Thus, our fiber-based interface offers an optimal

combination of high efficiency, compactness, scalability, and quantum fidelity, which are key components for deploying QFC technologies in practical quantum information processing architectures.

In conclusion, we demonstrated an efficient and coherent QFC interface compatible with the best-performing SPS, such as the NIR QD. We achieved a state-of-the-art end-to-end efficiency ($\eta_{ext} = 48.4\%$). We also report the preservation of unicity and indistinguishability, which are key parameters for the development of quantum information technologies. The fibered conversion stage ensures the compactness and transportability of the system, offering viable solutions for real field and deployed applications. This work paves the way for quantum key distribution (QKD) solutions, implementing one-way links based on single photons as qubit carriers [47] and extending to long-range networks to achieve quantum repeaters based on quantum state teleportation outside laboratory settings.

ACKNOWLEDGMENT

This work was conducted within the framework of the OPTIMAL project granted by the European Union by means of the Fond Européen de développement régional (FEDER). The authors also acknowledge the financial support from the Agence Nationale de la Recherche (ANR) through the projects LIGHT (18-ASTR-0024), the European Comission for the Quantera project (IN-QURE ANR-22-QUA1-0002) and the French government through its Investments for the Future program under the Université Côte d’Azur UCA-JEDI project (Quantum@UCA) managed by the ANR (ANR-15-IDEX-01).

AUTHOR INFORMATION

COMPETING INTERESTS

P. Senellart and N. Somaschi are co-founders, and the CEO and CSO of Quandela, respectively.

DATA AVAILABILITY

The data are available from the authors upon request.

[1] B. Costa, B. Scaparra, X. Wei, H. Riedl, G. Koblmüller, E. Zallo, J. Finley, L. Hanschke, and K. Müller, “Telecom quantum dots on GaAs substrates as integration-ready high performance single-photon sources,” arXiv:2505.22886 (2025).

[2] S. E. Thomas, M. Billard, N. Coste, S. C. Wein, Priya, H. Ollivier, O. Krebs, L. Tazaïrt, A. Harouri, A. Lemaitre, et al., “Bright polarized single-photon source based on a linear dipole,” Phys. Rev. Lett. **126**, 233601 (2021).

[3] N. Margaria, F. Pastier, T. Bennour, M. Billard, E. Ivanov, W. Hease, P. Stepanov, A. F. Adiyatullin, R. Singla, M. Pont, M. Descampeaux, A. Bernard, A. Pishchagin, M. Morassi, A. Lemaître, T. Volz, V. Giesz, N. Somaschi, N. Maring, S. Boissier, T. H. Au, and P. Senellart, “Efficient fiber-pigtailed source of indistinguishable single photons,” arXiv:2410.07760 (2024).

[4] N. Hauser, M. Bayerbach, J. Kaupp, Y. Reum, G. Penikov, J. Michl, M. Kamp, T. Huber-Loyola, A. T. Pfennig, S. Höfling, and S. Barz, “Deterministic and highly indistinguishable single photons in the telecom C-band,” arXiv:2505.09695 (2025).

[5] R. M. Pettit, S. Deckoff-Jones, A. Donis, A. Elias, J. Briscoe, G. Leake, D. Coleman, M. Fanto, A. Sundaresh, S. Gupta, M. K. Singh, and S. E. Sullivan, “Monolithically integrated C-band quantum emitters on foundry silicon photonics,” arXiv:2505.00224 (2025).

[6] X. Lu, Q. Li, D. A. Westly, G. Moille, A. Singh, V. Anant, and K. Srinivasan, “Chip-integrated visible–telecom entangled photon pair source for quantum communication,” Nat. Phys. **15**, 373 (2019).

[7] E. Arenskötter, T. Bauer, S. Kucera, M. Bock, J. Eschner, and C. Becher, “Telecom quantum photonic interface for a $^{40}\text{Ca}^+$ single-ion quantum memory,” arXiv:2211.08841 (2022).

[8] Q. Li, M. Davanço, and K. Srinivasan, “Efficient and low-noise single-photon-level frequency conversion interfaces using silicon nanophotonics,” Nat. Photonics **10**, 406 (2016).

[9] B. Jin, C. Yu, J. Yuan, X. Sang, X. Xiang, Z. Liu, and S. Wei, “Efficient wavelength conversion based on quasi-phase-matched four-wave mixing in a silicon waveguide with a microring phase shifter,” J. Opt. Soc. Am. B **30**, 2491 (2013).

[10] P. P. Absil, J. V. Hryniewicz, B. E. Little, P. S. Cho, R. A. Wilson, L. G. Joneckis, and P.-T. Ho, “Wavelength conversion in GaAs micro-ring resonators,” Opt. Lett. **25**, 554 (2000).

[11] K. De Greve, L. Yu, P. L. McMahon, J. S. Pelc, C. M. Natarajan, N. Y. Kim, E. Abe, S. Maier, C. Schneider, M. Kamp, S. Höfling, R. H. Hadfield, A. Forchel, M. M. Fejer, and Y. Yamamoto, “Quantum-dot spin–photon entanglement via frequency downconversion to telecom wavelength,” Nature **491**, 421 (2012).

[12] S. Ates, I. Agha, A. Gulinatti, I. Rech, M. T. Rakher, A. Badolato, and K. Srinivasan, “Two-photon interference using background-free quantum frequency conversion of single photons emitted by an InAs quantum dot,” Phys. Rev. Lett. **109**, 147405 (2012).

[13] V. R. Almeida, C. A. Barrios, R. R. Panepucci, and M. Lipson, “All-optical control of light on a silicon chip,” Nature **431**, 1081 (2004).

[14] A. Aghababaei, C. Biesek, F. Vewinger, and S. Stellmer, “Frequency conversion in high-pressure hydrogen,” Opt. Lett. **48**, 45 (2023).

[15] S. Clemmen, K. Phan Huy, W. Bogaerts, R. G. Baets, Ph. Emplit, and S. Massar, “Continuous-wave photon pair generation in silicon-on-insulator waveguides and ring resonators,” Opt. Express **17**, 16558 (2009).

[16] M. Cohen, A. Martin, R. Dalidet, F. Pastier, M. Billard, V. Giesz, N. Somaschi, S. Thomas, P. Senellart, S. Tanzilli, and L. Labonté, “A compact and efficient single-photon quantum frequency converter,” arXiv (2025), submitted.

[17] J. M. Donohue, M. D. Mazurek, and K. J. Resch, “Theory of high-efficiency sum-frequency generation for single-photon waveform conversion,” Phys. Rev. A **91**, 033809 (2015).

[18] M. A. Foster, A. C. Turner, R. Salem, M. Lipson, and A. L. Gaeta, “Broad-band continuous-wave parametric wavelength conversion in silicon nanowaveguides,” Opt. Express **15**, 12949 (2007).

[19] A. Hamer, S. M. R. Tabar, P. Yashwantrao, A. Aghababaei, F. Vewinger, and S. Stellmer, “Frequency conversion to the telecom O-band using pressurized hydrogen,” arXiv:2401.10003 (2024).

[20] T. J. Kippenberg, S. M. Spillane, and K. J. Vahala, “Kerr-nonlinearity optical parametric oscillation in an ultrahigh- Q toroid microcavity,” Phys. Rev. Lett. **93**, 083904 (2004).

[21] A. Lenhard, J. Brito, M. Bock, J. Eschner, and C. Becher, “Coherence and entanglement preservation of frequency-converted heralded single photons,” Opt. Express **25**, 11187 (2017).

[22] Q. Li, A. Singh, X. Lu, J. Lawall, V. Verma, R. Mirin, S. W. Nam, and K. Srinivasan, “Tunable quantum beat of single photons enabled by nonlinear nanophotonics,” arXiv:1905.01698 (2019).

[23] S. Murakami, R. Fujimoto, T. Kobayashi, R. Ikuta, A. Inoue, T. Umeki, and S. Miki, “Quantum frequency conversion using a 4-port fiber-pigtailed PPLN module,” Opt. Express **31**, 29271 (2023).

[24] S. Murakami, T. Kobayashi, S. Miki, H. Terai, T. Kodama, T. Sawaya, A. Ohtomo, H. Shimo, T. Yamamoto, and R. Ikuta, “Low-noise quantum frequency conversion with cavity enhancement of converted mode,” arXiv:2409.05408 (2024).

[25] J. R. Ong, R. Kumar, R. Aguinaldo, and S. Mookherjea, “Efficient CW four-wave mixing in silicon-on-insulator micro-rings with active carrier removal,” IEEE Photonics Technol. Lett. **25**, 1699 (2013).

[26] U. Pfister, D. Wendland, F. Hornung, L. Engel, H. Hüging, E. Herzog, P. Vijayan, et al., “Telecom wave-

length quantum dots interfaced with silicon-nitride circuits via photonic wire bonding," arXiv:2411.05647 (2024).

[27] L. Rickert, K. Żolnacz, D. A. Vajner, M. von Helversen, S. Rodt, S. Reitzenstein, H. Liu, *et al.*, "A fiber-pigtailed quantum dot device generating indistinguishable photons at GHz clock-rates," arXiv:2409.08982 (2024).

[28] M. J. Strain, C. Lacava, L. Meriggi, I. Cristiani, and M. Sorel, "Tunable Q -factor silicon microring resonators for ultra-low power parametric processes," *Opt. Lett.* **40**, 1274 (2015).

[29] P. C. Strassmann, A. Martin, N. Gisin, and M. Afzelius, "Spectral noise in frequency conversion from the visible to the telecommunication C-band," *Opt. Express* **27**, 14298 (2019).

[30] S. Tanzilli, W. Tittel, M. Halder, O. Alibart, P. Baldi, N. Gisin, and H. Zbinden, "A photonic quantum information interface," *Nature* **437**, 116 (2005).

[31] R. Tyumenev, J. Hammer, N. Y. Joly, P. St. J. Russell, and D. Novoa, "Tunable and state-preserving frequency conversion of single photons in hydrogen," *Science* **376**, 621 (2022).

[32] X. Wang, X. Jiao, B. Wang, Y. Liu, X.-P. Xie, M.-Y. Zheng, Q. Zhang, and J.-W. Pan, "Quantum frequency conversion and single-photon detection with lithium niobate nanophotonic chips," arXiv:2209.08484 (2022).

[33] S. Zaske, A. Lenhard, C. A. Keßler, J. Kettler, C. Hepp, C. Arend, R. Albrecht, *et al.*, "Visible-to-telecom quantum frequency conversion of light from a single quantum emitter," *Phys. Rev. Lett.* **109**, 147404 (2012).

[34] M. K. Alqedra, C.-T. Huang, W.-H. Chang, S. Hafouz, P. J. Poole, D. Dalacu, A. W. Elshaari, and V. Zwiller, "Indistinguishable single photons from nanowire quantum dots in the telecom O-band," arXiv:2503.12116 (2025).

[35] Y. Pelet, G. Sauder, M. Cohen, L. Labonté, O. Alibart, A. Martin, and S. Tanzilli, "Operational entanglement-based quantum key distribution over 50 km of field-deployed optical fibers," *Phys. Rev. Appl.* **20**, 044006 (2023).

[36] D. P. Nadlinger, P. Drmota, B. C. Nichol, G. Araneda, D. Main, R. Srinivas, D. M. Lucas, C. J. Ballance, K. Ivanov, E. Y.-Z. Tan, P. Sekatski, R. L. Urbanke, R. Renner, N. Sangouard, and J.-D. Bancal, "Experimental quantum key distribution certified by Bell's theorem," *Nature* **607**, 682 (2022).

[37] D. Cogan, Z.-E. Su, O. Kenneth, and D. Gershoni, "Deterministic generation of indistinguishable photons in a cluster state," *Nat. Photonics* **17**, 324 (2023).

[38] N. Coste, D. A. Fioretto, N. Belabas, S. C. Wein, P. Hilaire, R. Frantzeskakis, M. Gundin, B. Goes, N. Somaschi, M. Morassi, *et al.*, "High-rate entanglement between a semiconductor spin and indistinguishable photons," *Nat. Photonics* **17**, 582 (2023).

[39] H. Huet, P. R. Ramesh, S. C. Wein, N. Coste, P. Hilaire, N. Somaschi, M. Morassi, A. Lemaître, I. Sagnes, M. F. Doty, *et al.*, "Deterministic and reconfigurable graph state generation with a single solid-state quantum emitter," *Nat. Commun.* **16**, 4337 (2025).

[40] L. Labonté, O. Alibart, V. D'Auria, F. Doutre, J. Etesse, G. Sauder, A. Martin, É. Picholle, and S. Tanzilli, "Integrated photonics for quantum communications and metrology," *PRX Quantum* **5**, 010101 (2024).

[41] C. Nawrath, R. Joos, S. Kolatschek, S. Bauer, P. Pruy, F. Hornung, J. Fischer, J. Huang, P. Vijayan, R. Sittig, M. Jetter, S. L. Portalupi, and P. Michler, "High emission rate from a Purcell-enhanced, triggered source of pure single photons in the telecom C-band," arXiv:2207.12898 (2022).

[42] S. Murakami, T. Kobayashi, S. Miki, H. Terai, T. Kodama, T. Sawaya, A. Ohtomo, H. Shimo, T. Yamamoto, and R. Ikuta, "Low-noise quantum frequency conversion with cavity enhancement of converted mode," arXiv:2409.05408 (2024).

[43] L. R. Murphy, M. J. Olszewski, P. Androvitsaneas, M. A. Perez, W. A. M. Smith, A. J. Bennett, P. J. Mosley, and A. O. C. Davis, "Tunable frequency conversion in doped photonic crystal fiber pumped near degeneracy," *Optica* **11**, 1490 (2024).

[44] U. Pfister, D. Wendland, F. Hornung, L. Engel, H. Hüging, E. Herzog, P. Vijayan, R. Joos, E. Jung, M. Jetter, S. L. Portalupi, W. H. P. Pernice, and P. Michler, "Telecom wavelength quantum dots interfaced with silicon-nitride circuits via photonic wire bonding," arXiv:2411.05647 (2024).

[45] F. Kaiser, P. Vergyris, A. Martin, D. Aktas, M. P. De Micheli, O. Alibart, and S. Tanzilli, "Quantum optical frequency up-conversion for polarisation entangled qubits: towards interconnected quantum information devices," *Opt. Express* **27**, 25603 (2019).

[46] L. R. Murphy, M. J. Olszewski, P. Androvitsaneas, M. A. Perez, W. A. M. Smith, A. J. Bennett, P. J. Mosley, and A. O. C. Davis, "Tunable frequency conversion in doped photonic crystal fiber pumped near degeneracy," arXiv:2407.09266 (2024).

[47] C. L. Morrison, R. G. Pousa, F. Graffitti, Z. X. Koong, P. Barrow, N. G. Stoltz, D. Bouwmeester, J. Jeffers, D. K. L. Oi, B. D. Gerardot, *et al.*, "Single-emitter quantum key distribution over 175 km of fibre with optimised finite key rates," *Nat. Commun.* **14**, 3573 (2023).

[48] X. Wang, X. Jiao, B. Wang, Y. Liu, X.-P. Xie, M.-Y. Zheng, Q. Zhang, and J.-W. Pan, "Quantum frequency conversion and single-photon detection with lithium niobate nanophotonic chips," *npj Quantum Inf.* **9**, 38 (2023).

[49] H. Ollivier, S. E. Thomas, S. C. Wein, I. M. de Buy Weniger, N. Coste, J. C. Loredo, N. Somaschi, A. Harouri, A. Lemaître, and I. Sagnes, "Hong–Ou–Mandel interference with imperfect single photon sources," *Phys. Rev. Lett.* **126**, 063602 (2021).

[50] Y. Arakawa and M. J. Holmes, "Progress in quantum-dot single photon sources for quantum information technologies: A broad spectrum overview," *Appl. Phys. Rev.* **7**, 020902 (2020).

[51] P. Senellart, G. Solomon, and A. White, "High-performance semiconductor quantum-dot single-photon sources," *Nat. Nanotechnol.* **12**, 1026 (2017).

[52] N. Somaschi, V. Giesz, L. De Santis, J. C. Loredo, M. P. Almeida, G. Hornecker, S. L. Portalupi, T. Grange, C. Anton, J. Demory *et al.*, "Near-optimal single-photon sources in the solid state," *Nature Photonics* **10**, 340–345 (2016).

[53] J.-P. Chen, C. Zhang, Y. Liu, C. Jiang, D.-F. Zhao, W.-J. Zhang, F.-X. Chen, H. Li, L.-X. You, Z. Wang *et al.*, "Quantum key distribution over 658 km fiber with distributed vibration sensing," *Phys. Rev. Lett.* **128**, 180502 (2022).

[54] C. Nawrath, R. Joos, S. Kolatschek, S. Bauer, P. Pruy, F. Hornung, J. Fischer, J. Huang, P. Vijayan, R. Sittig et al., “High emission rate from a Purcell-enhanced, triggered source of pure single photons in the telecom C-band,” *arXiv:2207.12898* (2022).

[55] P. Komar, E. M. Kessler, M. Bishof, L. Jiang, A. S. Sørensen, J. Ye, and M. D. Lukin, “A quantum network of clocks,” *Nature Physics* **10**, 582–587 (2014).

[56] H.-J. Briegel, W. Dür, J. I. Cirac, and P. Zoller, “Quantum repeaters: the role of imperfect local operations in quantum communication,” *Phys. Rev. Lett.* **81**, 5932 (1998).

[57] S. Langenfeld, S. Welte, L. Hartung, S. Daiss, P. Thomas, O. Morin, E. Distante, and G. Rempe, “Quantum teleportation between remote qubit memories with only a single photon as a resource,” *Phys. Rev. Lett.* **126**, 130502 (2021).

[58] W. Pfaff, B. J. Hensen, H. Bernien, S. B. van Dam, M. S. Blok, T. H. Taminiau, M. J. Tiggelman, R. N. Schouten, M. Markham, D. J. Twitchen et al., “Unconditional quantum teleportation between distant solid-state quantum bits,” *Science* **345**, 532–535 (2014).

[59] S. Pironio, A. Acín, N. Brunner, N. Gisin, S. Massar, and V. Scarani, “Device-independent quantum key distribution secure against collective attacks,” *New J. Phys.* **11**, 045021 (2009).

[60] A. Acín, N. Brunner, N. Gisin, S. Massar, S. Pironio, and V. Scarani, “Device-independent security of quantum cryptography against collective attacks,” *Phys. Rev. Lett.* **98**, 230501 (2007).

[61] A. Singh, Q. Li, S. Liu, Y. Yu, X. Lu, C. Schneider, S. Höfling, J. Lawall, V. Verma, R. Mirin et al., “Quantum frequency conversion of a quantum dot single-photon source on a nanophotonic chip,” *Optica* **6**, 563–569 (2019).

[62] D. M. Lukin, M. A. Guidry, and J. Vučković, “Integrated quantum photonics with silicon carbide: challenges and prospects,” *PRX Quantum* **1**, 020102 (2020).

[63] B. Kambs, J. Kettler, M. Bock, J. N. Becker, C. Arend, A. Lenhard, S. L. Portalupi, M. Jetter, P. Michler, and C. Becher, “Low-noise quantum frequency down-conversion of indistinguishable photons,” *Opt. Express* **24**, 22250–22260 (2016).

[64] J. S. Pelc, L. Yu, K. De Greve, P. L. McMahon, C. M. Natarajan, V. Esfandyarpour, S. Maier, C. Schneider, M. Kamp, S. Höfling et al., “Downconversion quantum interface for a single quantum dot spin and 1550-nm single-photon channel,” *Opt. Express* **20**, 27510–27519 (2012).

[65] S. Zaske, A. Lenhard, C. A. Keßler, J. Kettler, C. Hepp, C. Arend, R. Albrecht, W.-M. Schulz, J. Michael, P. Michler et al., “Visible-to-telecom quantum frequency conversion of light from a single quantum emitter,” *Phys. Rev. Lett.* **109**, 147404 (2012).

[66] P. C. Strassmann, A. Martin, N. Gisin, and M. Afzelius, “Spectral noise in frequency conversion from the visible to the telecommunication C-band,” *Opt. Express* **27**, 14298–14307 (2019).

[67] A. Tchekbotareva, S. L. N. Hermans, P. C. Humphreys, D. Voigt, P. J. Harmsma, L. K. Cheng, A. L. Verlaan, N. Dijkhuizen, W. De Jong, A. Dréau et al., “Entanglement between a diamond spin qubit and a photonic time-bin qubit at telecom wavelength,” *Phys. Rev. Lett.* **123**, 063601 (2019).

[68] V. Krutyanskiy, M. Meraner, J. Schupp, V. Krcmarsky, H. Hainzer, and B. P. Lanyon, “Light-matter entanglement over 50 km of optical fibre,” *npj Quantum Information* **5**, 72 (2019).

[69] M. Bock, P. Eich, S. Kucera, M. Kreis, A. Lenhard, C. Becher, and J. Eschner, “High-fidelity entanglement between a trapped ion and a telecom photon via quantum frequency conversion,” *Nature Communications* **9**, 1998 (2018).

[70] Y. Yu, F. Ma, X.-Y. Luo, B. Jing, P.-F. Sun, R.-Z. Fang, C.-W. Yang, H. Liu, M.-Y. Zheng, X.-P. Xie et al., “Entanglement of two quantum memories via fibres over dozens of kilometres,” *Nature* **578**, 240–245 (2020).

[71] Y. O. Dudin, A. G. Radnaev, R. Zhao, J. Z. Blumoff, T. A. B. Kennedy, and A. Kuzmich, “Entanglement of light-shift compensated atomic spin waves with telecom light,” *Phys. Rev. Lett.* **105**, 260502 (2010).

[72] R. Ikuta, T. Kobayashi, T. Kawakami, S. Miki, M. Yabuno, T. Yamashita, H. Terai, M. Koashi, T. Mukai, T. Yamamoto et al., “Polarization insensitive frequency conversion for an atom-photon entanglement distribution via a telecom network,” *Nature Communications* **9**, 1997 (2018).

[73] E. Saglamyurek, J. Jin, V. B. Verma, M. D. Shaw, F. Marsili, S. W. Nam, D. Oblak, and W. Tittel, “Quantum storage of entangled telecom-wavelength photons in an erbium-doped optical fibre,” *Nature Photonics* **9**, 83–87 (2015).

[74] A. Lenhard, J. Brito, M. Bock, C. Becher, and J. Eschner, “Coherence and entanglement preservation of frequency-converted heralded single photons,” *Opt. Express* **25**, 11187–11199 (2017).

[75] B. Da Lio, C. Faurby, X. Zhou, M. L. Chan, R. Uppu, H. Thyrrstrup, S. Scholz, A. D. Wieck, A. Ludwig, P. Lodahl et al., “A pure and indistinguishable single-photon source at telecommunication wavelength,” *Adv. Quantum Technol.* **5**, 2200006 (2022).

[76] C. L. Morrison, M. Rambach, Z. X. Koong, F. Graffitti, F. Thorburn, A. K. Kar, Y. Ma, S.-I. Park, J. D. Song, N. G. Stoltz et al., “A bright source of telecom single photons based on quantum frequency conversion,” *Appl. Phys. Lett.* **118**, 17 (2021).

[77] S. Tanzilli, W. Tittel, M. Halder, O. Alibart, P. Baldi, N. Gisin, and H. Zbinden, “A photonic quantum information interface,” *Nature* **437**, 116–120 (2005).